

## Two-dimensional statistical model for regularized backprojection in SPECT

M Pélégri<sup>†</sup>, H Benali, I Buvat, G El Fakhri and R Di Paola

INSERM U66, CHU Pitié-Salpêtrière, 91, Boulevard de l'Hôpital, 75634 Paris Cédex 13, France

Received 19 March 1997, in final form 10 September 1997

**Abstract.** In SPECT, both the noise affecting the data and the discretization of the inverse Radon transform are responsible for the ill-posed nature of the reconstruction. To constrain the problem, we propose a regularized backprojection method (RBP) which takes advantage of the relationships existing between the continuity properties of the projections and those of the reconstructed object. The RBP method involves two stages: first, a statistical model (the fixed-effect model) is used to estimate the noise-free part of the projections. Then, the filtered projections are reconstructed using a backprojection algorithm (spline filtered backprojection) which ensures that the reconstructed object belongs to a space consistent with that containing the projections. The method is illustrated using analytical simulations, and the RBP approach is compared to the conventional filtered backprojection. The effect on the reconstructed slices of the parameters involved in RBP is studied in terms of spatial resolution, homogeneity in uniform regions and quantification. It is shown that appropriate combinations of these parameters yield a better compromise between homogeneity and spatial resolution than conventional FBP, with similar quantification performances.

### 1. Introduction

Tomographic reconstruction is a well known ill-posed inverse problem. Analytic reconstruction algorithms are derived from the Radon theory which applies to continuous signals (Radon 1917). However, the discrete inverse problem is unstable because the discrete inverse Radon operator does not present suitable properties of linearity and shift-invariance. Yet, it has been shown that the inverse Radon transform between appropriate regular spaces (Sobolev spaces) is continuous (Louis 1980, Natterer 1986): if the projections present the regularity properties which make them belong to a given Sobolev space, one can relate this space to the Sobolev space which the reconstructed object belongs to. In the following, this theorem will be termed the 'space correspondence theorem'.

In SPECT, in addition to the intrinsic discrete nature of the detected signal, noise also contributes to the ill-posedness of the reconstruction. Conventional approaches to tomographic reconstruction in the presence of noise include backprojecting filtered projections (Budinger *et al* 1979), modelling noise in iterative reconstruction schemes (Lange and Carson 1984) and using restoration filters such as the Wiener filter (see, e.g., King *et al* 1984). None of these methods, however, explicitly address the ill-posed nature of the reconstruction problem due to the signal discretization.

In this paper, we introduce a regularized backprojection method (RBP) to address the ill-posed nature of tomographic reconstruction in SPECT, by dealing with both the

<sup>†</sup> E-mail address: pelegri@imed.jussieu.fr

problems of noise and discretization. The aim of the RBP method is to ensure that the space correspondence theorem (relating the projection Sobolev space and the object Sobolev space) is satisfied. Using both the continuity and the statistical properties of the projections, a statistical model is proposed to estimate the noise-free part of the projections belonging to a given Sobolev space. The filtered projections are then reconstructed using the spline filtered backprojection algorithm (Guédon and Bizais 1991, 1994), which ensures that the reconstructed object belongs to the Sobolev space corresponding to the projection space.

Section 2 presents the theory underlying the regularized backprojection method. Sections 3 and 4 illustrate the method using analytical simulations, with a particular emphasis on how the parameters involved in the RBP affect the spatial resolution, the signal homogeneity in uniform regions and the absolute quantification in the reconstructed slices.

## 2. Theory

This section describes the regularized backprojection method, which takes advantage of the space correspondence theorem by means of two steps: a statistical model is first solved (sections 2.1 and 2.2) so that the noise affecting the tomographic data can be filtered while ensuring that the filtered projections belong to the desired Sobolev space. It is then shown (section 2.3) that performing the reconstruction using the spline filtered backprojection algorithm leads to an object belonging to the Sobolev space consistent with the projection space.

### 2.1. Statistical model for noise filtering

The filtering procedure is based upon an additive model called the fixed-effect model (Caussinus 1986), initially proposed in the statistical field of multidimensional data analysis. In a previous paper (Benali *et al* 1994), we described how the fixed-effect model could be used to deal with noisy tomographic data. In this paper, the model is specifically adapted to SPECT in the framework of the space correspondence theorem, and uses both the continuity and the statistical properties of the acquired projections as *a priori* knowledge.

*2.1.1. Fixed-effect model.* For a given slice, let  $P$  be the  $(N, T)$  acquired sinogram, where  $N$  is the number of projections and  $T$  is the number of bins per 1D projection. The elements of  $P$  are denoted by  $P_{ik}$ , where  $i = 1, N$  and  $k = 1, T$ . The  $T$ -vector  $P_i$  represents the variation of the signal along the bins within the projection  $i$ .

A tomographic acquisition device is characterized by a finite spatial response function. If there were no noise, the acquired projections should therefore be continuous functions along the projection bins, sampled at a number  $T$  of projection bins. The intrinsic regularity of  $P_{ik}$  along the bins of projections  $k$  can be modelled by assuming that  $P_i$  belongs to the Sobolev vector space  $H^{(m)}$ . The Sobolev space  $H^{(m)}$ ,  $m$  real, is defined as a space of functions having absolutely continuous derivatives up to order  $m - 1$ , and such that the square of the  $m$ th derivative has a finite integral (Adams 1975).

The fixed-effect model is defined in a Sobolev space as follows.

(1) The vectors  $P_i$  are defined on a probability space and can be written

$$P_i = \hat{P}_i + E_i$$

where  $\hat{P}_i$  is the non-random part (fixed part) of  $P_i$ , and  $E_i$  is a random error. In this model, the fixed part  $\hat{P}_i$  represents the noise-free projections.

(2) The random errors  $E_i$  are assumed not to depend on  $\hat{P}_i$ , i.e., the expectation of  $P_i$  is given by

$$E[P_i] = \hat{P}_i.$$

(3) The random errors  $E_i$  are also assumed to be independent from one projection to another. For any projection  $i$ , the variance of  $E_i$  along  $k$  can be written

$$E[E_i^t E_i] = \frac{1}{N} \Gamma$$

where  $t$  denotes the transpose and  $\Gamma$  is the covariance matrix of errors, which is supposed to be known and not to depend on  $i$ .  $\Gamma$  is a  $(T, T)$  symmetric positive definite matrix.

(4) There is a  $Q$ -dimensional subspace  $H_Q^{(m)}$  of  $H^{(m)}$  ( $Q < T$ ) such that all  $\hat{P}_i$  belong to  $H_Q^{(m)}$ .

In summary, the fixed-effect model assumes that the noise-free part of the signal belongs to a subspace of the space which the acquired signal belongs to. It models the continuity properties of the data by means of the Sobolev space  $H^{(m)}$  and assumes that the first- and the second-order properties of the noise are known.

*2.1.2. Properties of the noise.* In SPECT, noise is distributed according to Poisson statistics. Consequently, the covariance matrix of the errors  $E_i$  depends on  $i$ . As the fixed-effect model assumes that  $\Gamma$  does not depend on  $i$ , the following square root transform of the acquired data  $P_i$  is performed:

$$P_{ik} \mapsto \sqrt{P_{ik} + \frac{3}{8}}.$$

This conventional transformation changes a Poisson variable into an asymptotic Gaussian variable with a known asymptotic variance. The covariance matrix  $\Gamma$  should not depend on  $i$  any more and is given by (Rao 1985)

$$\Gamma \approx \frac{1}{4} I$$

where  $I$  is the  $(T, T)$  identity matrix.

## 2.2. Solution of the model

To solve the fixed-effect model, the subspace  $H_Q^{(m)}$  containing the noise-free part  $\hat{P}_i$  of the data  $P_i$  must be estimated. The noise-free sinogram is then given by the projection of  $P_i$  onto the subspace  $H_Q^{(m)}$ .

*2.2.1. Determining  $H_Q^{(m)}$ .* As shown by Besse (1988), the least-square estimate of  $H_Q^{(m)}$  is obtained by minimizing the expression

$$\mathfrak{N} = \frac{1}{N} \sum_{i=1}^N E \left[ |P_i^\gamma - \hat{P}_i|_{\Gamma^{-1}}^2 \right] \quad (1)$$

where  $P_i^\gamma \in H^{(m)}$  is the smoothed version of  $P_i$ , and is the solution of

$$P_i^\gamma = \arg \inf_{h \in H^{(m)}} \left\{ \sum_{k=1}^T [P_{ik} - h_k]^2 + \gamma \sum_{k=1}^T h_k^{(m)} \Delta k \right\}. \quad (2)$$

$\Delta k$  is the size of a projection bin,  $h$  is a function of  $H^{(m)}$  with samples  $h_k$  and  $h^{(m)}$  is its  $m$ th derivative. It should be noted that expression (2) represents a trade-off between the

fidelity to the data  $P_i$ , as represented by the first term, and the smoothness of the solution, as represented by the second term.  $\gamma > 0$  is the smoothing parameter controlling this trade-off between fidelity and smoothness (Besse 1988). Schoenberg (1964) showed that the solution  $P_i^\gamma$  of equation (2) is a spline function, piecewise polynomial of degree  $2m - 1$ , in each interval  $[k, k + 1]$ , with the pieces joined at the knots  $k$  so that  $h$  has  $2m - 2$  continuous derivatives. For instance, cubic spline functions, piecewise polynomials of degree three, are obtained with  $m = 2$ .

The solution of the minimization problem given by equation (1) is obtained using a Principal Component Analysis of smoothing spline functions, involving the eigendecomposition of the matrix  $W\Gamma^{-1}$  (Caussinus 1986, Benali *et al* 1994);  $W$  is the  $(T, T)$  covariance matrix calculated by

$$W = \frac{1}{N}(P^\gamma - \bar{P}^\gamma)^\dagger(P^\gamma - \bar{P}^\gamma)$$

where the elements of the matrix  $P^\gamma$  are the  $P_{ik}^\gamma$ , and the elements of the mean matrix  $\bar{P}^\gamma$  are the  $\bar{P}_{ik}^\gamma$  defined by

$$\bar{P}_{ik}^\gamma = \frac{1}{N} \sum_{i'=1}^N P_{i'k}^\gamma.$$

The subspace  $H_Q^{(m)}$  is then spanned by the mean projection  $\bar{P}^\gamma$  and the first  $Q$  eigenvectors  $U_k^q$  associated with the largest  $Q$  eigenvalues  $\lambda_q$  of the matrix  $W\Gamma^{-1}$ .

*2.2.2. Estimating the noise-free sinogram.* The orthogonal projection of  $P_i^\gamma$  onto the subspace  $H_Q^{(m)}$  leads to the filtered sinogram  $\tilde{P}_i^\gamma$  estimating the noise-free sinogram  $\hat{P}_i$ :

$$\tilde{P}_{ik}^\gamma = \bar{P}_{ik}^\gamma + \sum_{q=1}^Q \sqrt{\lambda_q} V_i^q U_k^q$$

where the principal components  $V_i^q$  are given by

$$V_i^q = \frac{1}{\sqrt{\lambda_q}} \sum_{k=1}^T ([P_{ik}^\gamma - \bar{P}_{ik}^\gamma] U_k^q).$$

The final filtered sinogram is then obtained by performing the inverse transform:

$$\tilde{P}_{ik}^\gamma \mapsto [\tilde{P}_{ik}^\gamma]^2 - \frac{3}{8}.$$

It should be noted that if  $\tilde{P}_i^\gamma$  belongs to  $H^{(m)}$ ,  $[\tilde{P}_i^\gamma]^2$  also belongs to  $H^{(m)}$ . As the final projection space is known, the space correspondence theorem can be applied.

### 2.3. Reconstruction model

The fixed-effect model not only deals with the problem of noise, but also allows the first condition of the space correspondence theorem to be satisfied by ensuring that the filtered projections belong to a Sobolev space. However, reconstruction from noise-free projections remains an ill-posed problem because of the finite number of projections. Yet, the space correspondence theorem states that the inverse Radon transform between appropriate Sobolev spaces is continuous and, more precisely, that the inverse Radon transform of a set of projections belonging to  $H^{(m)}$  is an object belonging to  $H^{(m-1/2)}$  (Louis 1980, Natterer 1986). As the projections  $\tilde{P}_i^\gamma$  were modelled with spline functions of order  $2m - 1$ , it follows that the object belonging to  $H^{(m-1/2)}$  can be modelled with spline functions of order  $2m - 2$ .

The reconstruction problem is then no longer ill-posed, provided that the continuous inverse Radon transform is discretized in such a way that the linearity and shift-invariance properties of the continuous operator are maintained (Guédon and Bizais 1991).

The spline filtered backprojection (SFBP) algorithm proposed by Guédon and Bizais (1991, 1994) was initially developed to account for the relationships existing between the continuous and discrete versions of the standard FBP reconstruction method. It operates slice by slice (i.e., 2D reconstruction) and forces the reconstructed object to belong to a function space in which the inverse Radon transform is continuous, e.g., a Sobolev space. We adapted this method to reconstruct an object belonging to  $H^{(m-1/2)}$ . The SFBP algorithm then derives the optimal spline ramp filter, which consists of the convolution of the infinite ramp filter with spline functions of order  $2m - 2$ .

The projections  $\tilde{P}_i^\gamma$  are filtered using this optimal spline ramp filter and then backprojected to obtain the reconstructed object belonging to  $H^{(m-1/2)}$ . The SFBP algorithm is therefore a straightforward method to be used for the reconstruction of an object belonging to the desired Sobolev space. The combination ‘filtering/SFBP’ performed in consistent Sobolev spaces is what we call the regularized backprojection (RBP).

Figure 1 gives a synopsis of the processing steps, from the acquired data to the reconstructed object. In summary, RBP requires two steps: a noise filtering procedure followed by a consistent reconstruction algorithm (SFBP). Three parameters in total are involved in the noise filtering step: the projection Sobolev space dimension  $m$ , the smoothing parameter  $\gamma$  (equation (2)) and the dimension  $Q$  of the Sobolev subspace  $H_Q^{(m)}$ .

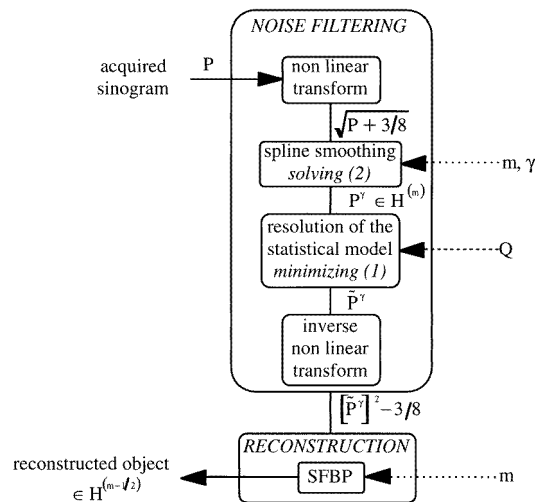


**Figure 1.** Regularized filtered backprojection (RBP): summary of the processing steps. The dotted arrows show the steps in which parameters are involved.

### 3. Materials and methods

#### 3.1. Data simulation

The effectiveness of the proposed approach was assessed using analytical simulations. All phantoms described below consisted of a single cross-section generated using the RECLBL library (Huesman *et al* 1977). In each case 128 equally spaced projections along a  $360^\circ$

circular orbit were calculated for a parallel geometry, with 128 bins per projection, using a projector of the RECLBL library. The projector did not take into account attenuation nor scatter, but was modified to account for a depth-dependent detector response function corresponding to that of an LEHR collimator. The detector response was assumed to be a symmetric Gaussian function with a standard deviation varying linearly with the source depth. The pixel size was 4.14 mm. Poisson noise was added to the calculated projections.

**3.1.1. Homogeneity and spatial resolution phantom.** A first simulation was conducted to study how the spatial resolution and the signal homogeneity in uniform regions would change when filtering the sinogram with different  $\gamma$  and  $Q$  values. The phantom was a homogeneous ellipse including nine one-pixel spots (figure 2(a)). The spots:background count ratio was 20:1. The mean number of counts per pixel in the resulting noisy sinogram was approximately 150.

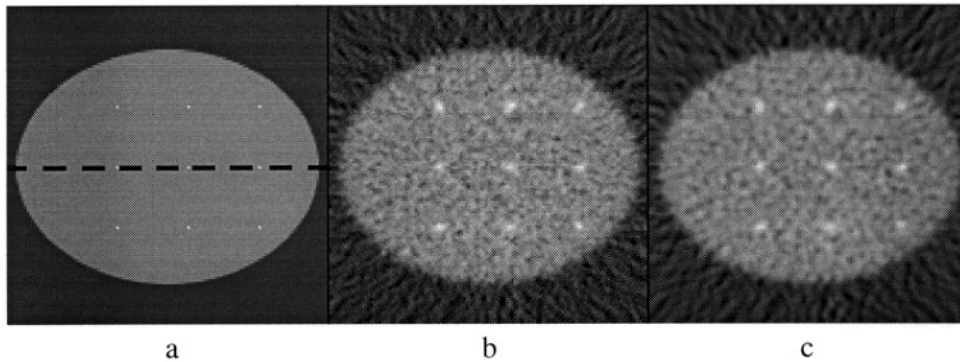


**Figure 2.** (a) Simulated spatial resolution phantom; the straight line represents the level of the horizontal profile shown in figure 7. (b) Reconstructed slice obtained with FBP-HAN. (c) Reconstructed slice obtained with RBP [ $\gamma = 10^{-4}$ ,  $Q = 45$ ].

**3.1.2. Quantification phantom.** An elliptical phantom was generated with homogeneous regions of various count levels large enough to avoid partial volume effects and to perform statistical tests between ROIs (figure 3(a)). The noisy sinogram resulting from this numerical simulation is shown in figure 3(b). The mean number of counts per pixel in that sinogram was approximately 90.

### 3.2. Data analysis

**3.2.1. Image reconstruction.** The following reconstruction schemes were compared:

(1) filtered backprojection (FBP) using the conventional Hann (FBP-HAN, cut-off frequency:  $0.5 \text{ pixel}^{-1}$ ) and Butterworth filters (order: 4, cut-off frequency:  $0.25 \text{ pixel}^{-1}$ ) (as the reconstructed images with these two filters were never significantly different, only the FBP-HAN results are presented in section 4) and

(2) regularized backprojection (RBP) with  $\gamma$  varying from  $10^{-7}$  to  $10^{-2}$  and  $Q$  varying from 10 to 50. Cubic spline filters were used to model the continuity of the projections (i.e.,  $m = 2$ ), and the spline filter used to reconstruct the object was calculated using quadratic spline functions to be consistent with the spline reconstruction model.

Depth-dependent blurring was not compensated for.

3.2.2. *Homogeneity and spatial resolution phantom.* For the spatial resolution phantom, the variance was calculated in a large region of interest (238 pixels) drawn in the background ellipse to characterize the signal homogeneity in the reconstructed background.

As the size of the simulated spots was smaller than twice the FWHM of the detector response function, the number of counts measured at the theoretical centre of the spot was directly related to the real size of the reconstructed spot (Hoffman *et al* 1979), i.e., to the spatial resolution in the reconstructed image. The spatial resolution was therefore characterized by measuring the number of counts at the centre of the spots as a function of  $\gamma$  and  $Q$ . The same measures were performed on the FBP images.

3.2.3. *Quantification phantom.* The reconstructions were normalized to ensure that the total number of counts in the reconstructed slice was equal to the total number of counts in the sinogram, so that absolute quantitative analysis could be performed. The average number of events per pixel and the corresponding standard deviation were calculated in four rectangular ROIs (238 pixels each) with intrinsic uniform count density (figure 3(c)).

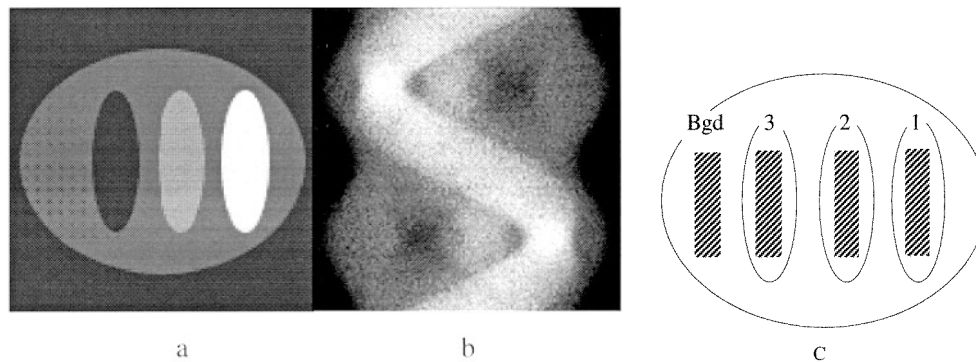


**Figure 3.** (a) Simulated quantification phantom with the region:background concentration ratios equal to 0:1, 2:1, 4:1 from left to right. (b) Noisy sinogram. (c) Regions of interest used for absolute quantification.

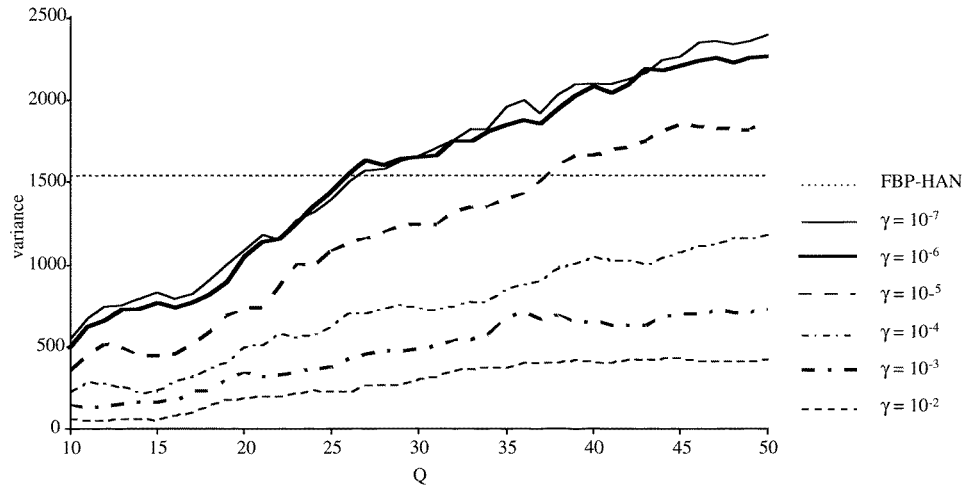
## 4. Results

### 4.1. Homogeneity and spatial resolution phantom

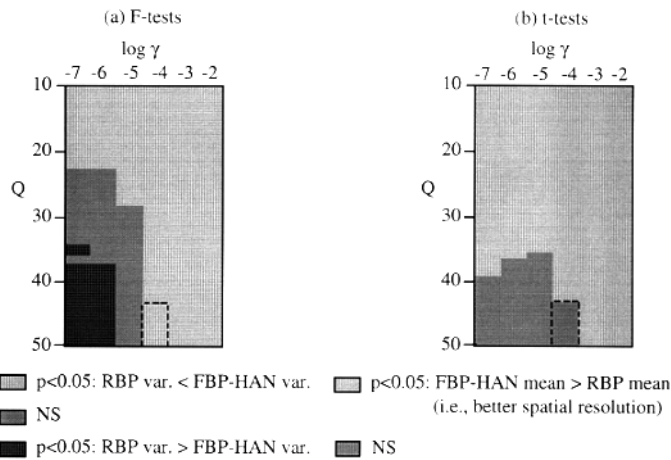
Figure 4 shows the variance values measured in the background ROI, for different  $\gamma$  and  $Q$  values. As expected, the higher  $\gamma$  and the lower  $Q$ , the more homogeneous the background signal. *F*-tests comparing the variance values in the background ROI obtained using RBP and FBP-HAN reconstructions are summarized in figure 5(a). The lightest area corresponds to the  $[\gamma, Q]$  combinations for which the background signal in the RBP images was more homogeneous than the background signal in the FBP-HAN images.

Figure 6 shows the mean number of counts calculated over the nine points in the reconstructed images; as previously mentioned, due to the partial volume effect, this mean count level characterized a mean spatial resolution in the images. The higher  $\gamma$  and the lower  $Q$ , the lower the number of counts, i.e., the worse the spatial resolution.

Results of the *t*-tests comparing the mean count level obtained using RBP reconstructions and FBP-HAN reconstruction are summarized in figure 5(b). The darkest area corresponds

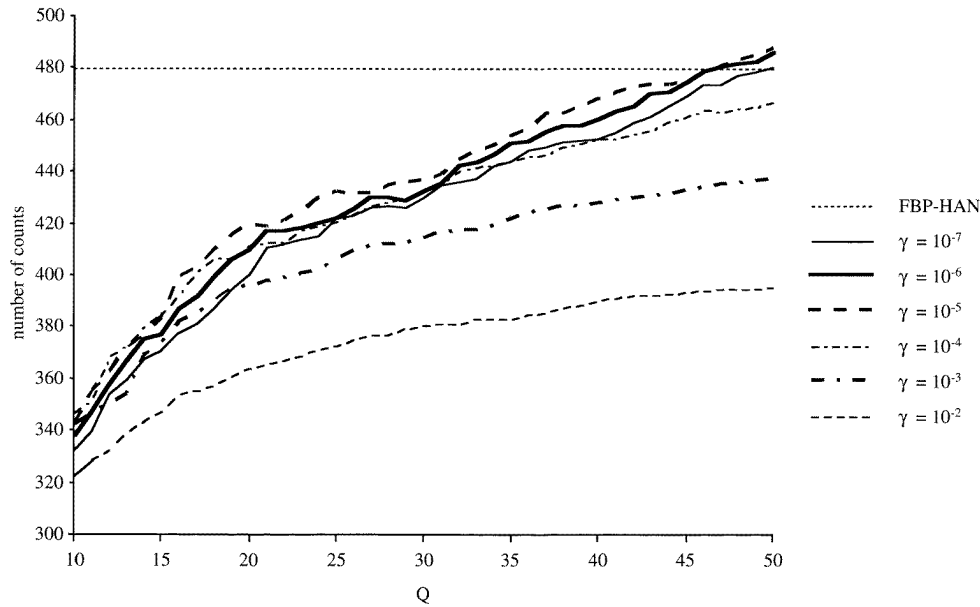


**Figure 4.** Variance values measured in the background ROI of the spatial resolution phantom as a function of  $Q$  and  $\gamma$ .

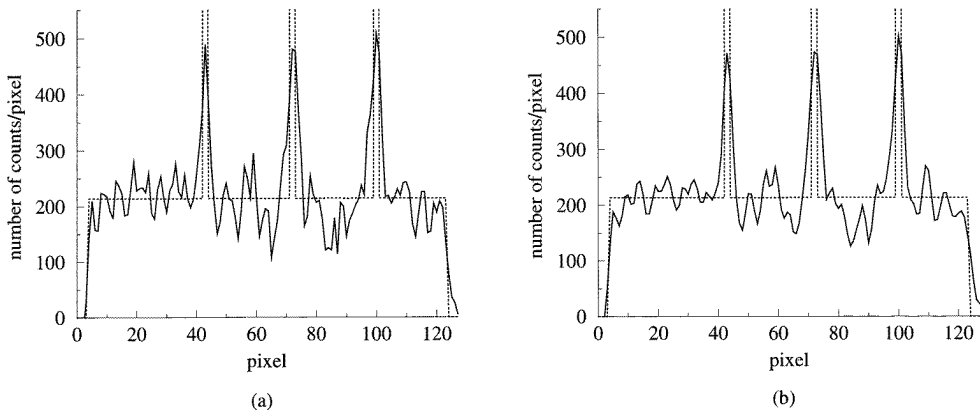


**Figure 5.** Results of the statistical tests for the spatial resolution phantom. (a)  $F$ -tests comparing RBP variance in the background ROI with FBP-HAN variance. (b)  $t$ -tests comparing RBP mean count level over the nine points with FBP-HAN mean count level. The area inside the dashed line represents the  $[\gamma, Q]$  combination yielding a greater background homogeneity with no significant loss in spatial resolution.

to the  $[\gamma, Q]$  values for which the spatial resolution in the RBP images is as good as for the FBP-HAN images. Combining the results of the  $F$ -tests and  $t$ -tests given in figure 5 showed that the choice  $[\gamma = 10^{-4}, Q \geq 45]$  led to a reconstruction where the background signal was more homogeneous than with a conventional FBP-HAN reconstruction, with no significant loss in spatial resolution. This result can be clearly seen on the horizontal profile drawn through the central spots (figure 7) for the FBP-HAN reconstruction and the RBP  $[\gamma = 10^{-4}, Q = 45]$  reconstruction. Figures 2(b) and 2(c) show the corresponding reconstructed slices.



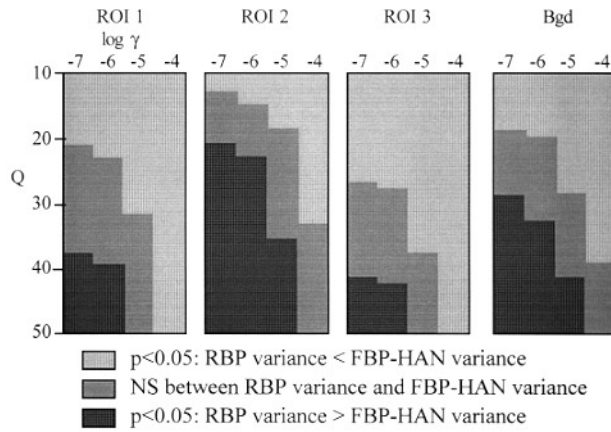
**Figure 6.** Mean count level over the nine reconstructed spots in the spatial resolution phantom as a function of  $Q$  and  $\gamma$ .



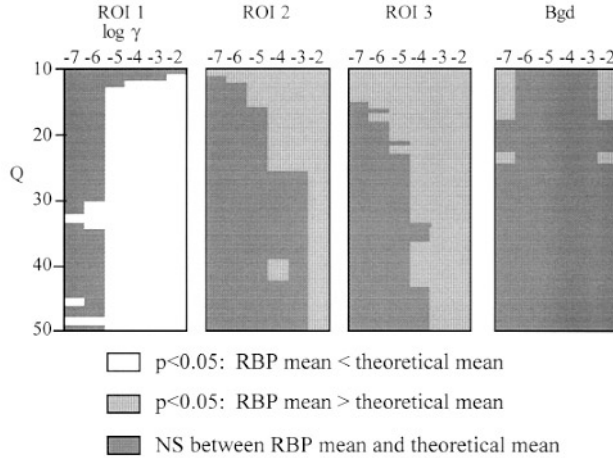
**Figure 7.** Dotted line: theoretical horizontal profile through the central spots of the spatial resolution phantom. Solid line: corresponding profiles obtained on the reconstructed slices using FBP-HAN (a) and RBP [ $\gamma = 10^{-4}$ ,  $Q = 45$ ] (b).

#### 4.2. Quantification phantom

Figure 8 summarizes the results obtained when comparing the variance values measured in ROIs drawn on the FBP-HAN and RBP images. For all  $Q$  values, the variance with  $\gamma \geq 10^{-3}$  was significantly lower than the variance obtained with FBP-HAN and the corresponding values were not represented for clarity. The lightest areas correspond to the  $[\gamma, Q]$  values for which the variance values in the ROIs were significantly lower in RBP images than in FBP-HAN images.



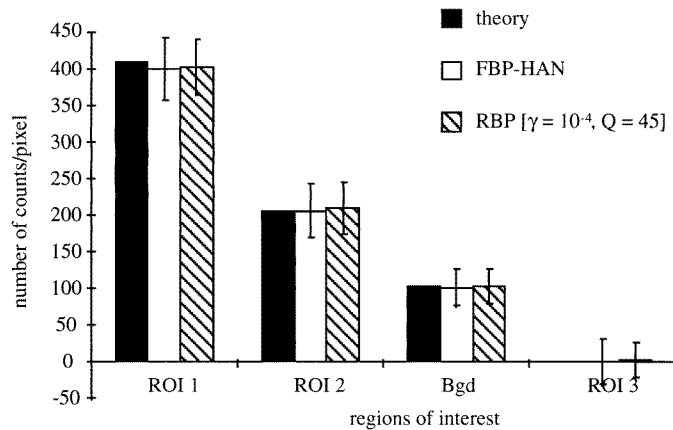
**Figure 8.** Results of the  $F$ -tests comparing the variance values measured in the RBP reconstructed slice with those measured in the FBP-HAN reconstructed slice.



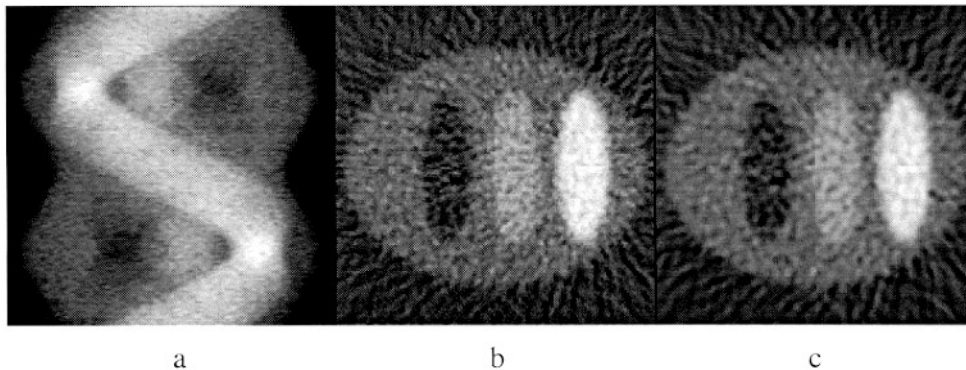
**Figure 9.** Results of the  $Z$ -tests comparing the mean values in the RBP reconstructed slice with the theoretical mean.

Figure 9 summarizes the results of the  $Z$ -tests comparing the means in the ROIs drawn on RBP images with the theoretical values. The darkest areas correspond to  $[\gamma, Q]$  values for which the count level in the RBP ROIs was correctly restored. FBP-HAN mean was significantly lower than the theoretical mean in ROI 1 ( $p < 0.05$ ), but not significantly different in the other ROIs.

In summary, the choice  $[\gamma = 10^{-4}, Q \geq 45]$  yielded a reconstruction where absolute quantification was equivalent to that obtained with FBP-HAN, but with a significantly lower variance in ROIs 1 and 3. Figure 10 shows the count level values obtained for the FBP-HAN and RBP  $[\gamma = 10^{-4}, Q = 45]$  reconstructions; the corresponding reconstructed slices are shown in figure 11.



**Figure 10.** Mean  $\pm 1$  standard deviation measured in the ROIs for the quantification phantom.



**Figure 11.** (a) Filtered sinogram of the quantification phantom with [ $\gamma = 10^{-4}$ ,  $Q = 45$ ]. Reconstructed slices obtained using FBP-HAN (b) and RBP [ $\gamma = 10^{-4}$ ,  $Q = 45$ ] (c).

## 5. Discussion

There are basically two reasons for the ill-posed nature of tomographic reconstruction in general, and in SPECT in particular: the noise affecting the acquired data and the discretization of the inverse Radon transform. In this paper, we propose a regularized backprojection method addressing both problems. We show that these two issues can be consistently dealt with by applying the space correspondence theorem.

Noise is dealt with using the fixed-effect model, which permits us to account for two kinds of *a priori* knowledge: (1) SPECT events are Poisson distributed; (2) noise-free projections should intrinsically present a certain regularity because of the limited spatial resolution of the imaging system. This model describes the projections as a linear combination of a noise-free component and an error. As the model assumes that the covariance of the error does not depend on the projections, a square-root transform of the initial SPECT data is first used; the covariance matrix of the resulting errors should then not depend on the projections any more ( $\Gamma \approx 0.25I$ ). The model also assumes that the data belong to a Sobolev space, consistent with the fact that the projections should present a

certain regularity or smoothness due to the limited spatial resolution of the imaging system. Projecting the data onto the Sobolev space involves using spline functions, with an order to be determined. In this study, a Sobolev space of order  $m = 2$  was chosen: cubic splines are mainly used because they are easily calculated (Harwell 1990) and give in general satisfactory results (Reinsch 1967). The fixed-effect model in Sobolev space is solved using a Principal Component Analysis to estimate the noise-free part of the projections. Solving the fixed-effect model in a Sobolev space after the square-root transformation is equivalent to a non-linear filtering of the original projections. It has been shown that this approach leads to a better estimation of the noise-free sinogram than spline smoothing alone or linear filtering alone (Benali *et al* 1994).

To deal with the ill-posed nature of the reconstruction, the discretization of the inverse Radon transform was optimized by performing the reconstruction of the filtered projections using the SFBP algorithm. The relevance of adding continuity constraints in the spline ramp filter was discussed by Guédon and Bizais (1991, 1994). In this paper, we pointed out that this method could be used in the particular context of the space correspondence theorem; the main point is that in the framework of the space correspondence theorem, choosing the spline order  $m$  involved in the fixed-effect model completely determines the filter to be used for the reconstruction: using cubic splines ( $m = 2$ ) in the fixed-effect model implies using quadratic splines for the reconstruction filter (see figure 1).

In addition to the spline order, two other parameters must be chosen when solving the fixed-effect model: (1) the smoothing parameter  $\gamma$  used when fitting the projections using spline functions: the higher  $\gamma$ , the smoother the projections, as illustrated by the numerical simulations (in that respect,  $1/\gamma$  is analogous to the cut-off frequency of the ramp filter (Wahba 1990)); (2) the second parameter is the dimension  $Q$  of the Sobolev subspace.  $Q$  represents the dimension of the subspace containing the noise-free component. The smaller  $Q$ , the greater the filtering; in other words, the higher  $Q$ , the better the spatial resolution in the reconstructed image.

The challenge is therefore to determine a combination of  $[\gamma, Q]$  which will actually remove noise without losing any relevant information. This challenge is similar to determining the appropriate cut-off frequency and/or order of a filter when using conventional FBP, or the regularization parameter in iterative schemes. Several methods have been suggested for choosing  $Q$  (Besse 1988, Wold 1978), or the combination  $[\gamma, Q]$  using cross-validation methods (Craven and Wahba 1979). In the case of Principal-Component Analysis, however, the theory of perturbations showed that the cross-validation methods are the same than those using conventional criteria (Besse and Ferre 1993), such as percentage of explained variance described by Jolliffe (1986). For the spatial resolution phantom and the quantification phantom presented in this study, the percentage of explained variance ranged from 95% to 99.8% for  $10 \leq Q \leq 50$  and did not prove to be useful to determine the appropriate  $Q$  value. Nevertheless, the numerical experiments reported in this paper showed that, for the simulated phantoms, it was possible to find a  $[\gamma, Q]$  combination yielding a better trade-off between signal homogeneity in uniform regions, count level restoration and spatial resolution than that with a conventional FBP reconstruction. The aim of this paper was mainly to describe a consistent reconstruction theory and to assess its feasibility. The method was thus only compared with FBP using conventional filters (Hann  $f_c = 0.5 \text{ pixel}^{-1}$  and Butterworth, order 4,  $f_c = 0.25 \text{ pixel}^{-1}$ ) because (1) the SFBP reconstruction method was initially developed to improve standard FBP reconstruction; (2) FBP is the most commonly used method in clinical practice. Further work is necessary to determine whether there is always a  $[\gamma, Q]$  combination that would provide a better 'noise/quantification/spatial resolution' trade-off than optimized FBP reconstructions, for any

object and noise level. Moreover, as the filtering method models the statistical properties of the signal, RBP should also be compared with other reconstruction methods taking the statistical properties of the data into account, such as ML-EM. Performing the RBP reconstruction took about 30 s using a Ultra1 SunSPARC workstation, while an FBP-HAN reconstruction took about 7 s. However, the RBP algorithm could be optimized to run faster.

In the spatial resolution phantom, a mean number of counts was calculated over the nine spots to characterize the spatial resolution using the partial volume effect. This calculation was relevant because the count level of every spot behaved the same way for the different  $[\gamma, Q]$  combinations. The differences between the spots, mainly shape differences, were not considered individually in this study.

Quantification in ROI 1 of the quantification phantom showed that the count level was significantly different from the theoretical value. The same experiment was conducted without simulating the detector response function, and the mean count level in ROI 1 was not significantly different from the theoretical mean. This emphasizes the necessity of compensating for the depth-dependent blurring to achieve accurate quantification.

In this paper, the method was validated using simulated projections where only the detector response and the acquisition noise were modelled. However, the RBP method has already been applied to the reconstruction of attenuation maps from short-duration transmission tomographic acquisitions. Indeed, the statistical properties and continuity properties of transmission projections are the same as those of emission projections (Pélegrini *et al* 1996). We are also currently applying the method to Monte Carlo simulations, which are corrupted by noise, attenuation, scatter and variable geometric point spread function. A whole protocol involving RBP and allowing for scatter, variable point spread function and attenuation compensation is under investigation (El Fakhri *et al* 1997).

## 6. Conclusion

In SPECT, both the noise affecting the data and the discretization of the inverse Radon transform make the problem of reconstruction ill-posed. In this paper, we showed that these two issues could be consistently dealt with in the framework of the space correspondence theorem, using a regularized backprojection method. Noise-free projections belonging to a given Sobolev space are first estimated using the fixed-effect model. The SFBP algorithm is then used to obtain a reconstructed object belonging to the Sobolev space consistent with the projection Sobolev space, according to the space correspondence theorem. In addition to the Sobolev space dimension, the model involves two parameters. The respective influence of these parameters was studied using numerical simulations. An optimal way to determine their values is still under investigation. The feasibility of the method has been shown and the RBP approach has been compared to conventional FBP results. Further studies will include the detailed comparison with different reconstruction algorithms and the extension of the two-dimensional model to full three-dimensional reconstruction.

## Acknowledgments

The authors thank J P Guédon for implementing the SFBP algorithm. M Pélegrini and G El Fakhri thank the 'Institut de Formation Supérieure Biomédicale' (Villejuif, France) and Sopha Medical Vision International (Buc, France) for supporting their PhDs.

## References

- Adams R 1975 *Sobolev Spaces* (New York: Academic)
- Benali H, Guédon J P, Buvat I, Pélégriani M, Bizais Y and Di Paola R 1994 A statistical model for tomographic reconstruction methods using spline functions *Proc. SPIE* **2299** 242–51
- Besse P 1988 Spline functions and optimal metric in linear principal component analysis *Component and Correspondence Analysis* ed J L A Van Rijckevorsel and J De Leeuw (London: Wiley) pp 81–103
- Besse P and Ferre L 1993 Sur l'usage de la validation croisée en analyse en composantes principales *Revue Stat. Appl.* **41** 71–6
- Budinger T F, Gullberg G T and Huesman R H 1979 Emission computed tomography *Image Reconstruction from Projections, Implementation and Applications* ed G T Herman (Berlin: Springer) pp 147–246
- Caussinus H 1986 Models and uses of principal component analysis *Multidimensional Data Analysis* ed J De Leeuw (Leiden: DSWO) pp 149–70
- Craven P and Wahba G 1979 Smoothing noisy data with spline functions. Estimating the correct degree of smoothing by the method of generalized cross-validation *Numer. Math.* **31** 377–403
- El Fakhri G, Buvat I, Pélégriani M, Almeida P, Benali H, Bendriem B and Di Paola R 1997 Propagation of errors due to scatter correction in cardiac SPECT reconstruction: a Monte Carlo study *Eur. J. Nucl. Med.* **24** 1035
- Guédon J P and Bizais Y 1991 Spline-based regularisation for discrete FBP reconstruction *12th IPMI Conf. (Wye, UK, 1991)* ed A C F Colchester and D J Hawkes (New York: Springer) pp 59–67
- 1994 Bandlimited and Haar filtered back-projection reconstructions *IEEE Trans. Med. Imaging* **13** 430–40
- Harwell 1990 *Harwell Subroutine Library Release 10—Specifications* (AEA Industrial Technology Harwell Laboratory)
- Hoffman E J, Huang S C and Phelps M E 1979 Quantitation in positron emission computed tomography: 1. Effect of object size *J. Comput. Assist. Tomogr.* **3** 299–308
- Huesman R H, Gullberg G T, Greenberg W L and Budinger T F 1977 RECLBL library users manual: Donner algorithms for reconstruction tomography *University of California Lawrence Berkeley Laboratory Publication* 214
- Jolliffe I T 1986 *Principal Component Analysis* (New York: Springer) pp 92–114
- King M A, Schwinger R B, Doherty P W and Penney B C 1984 Two-dimensional filtering of SPECT images using the Metz and Wiener filters *J. Nucl. Med.* **25** 1234–40
- Lange K and Carson R 1984 EM reconstruction algorithms for emission and transmission tomography *J. Comput. Assist. Tomogr.* **8** 306–16
- Louis A K 1980 Approximation of the Radon transform from samples in limited range *Mathematical Aspects of Computerized Tomography* ed G T Herman and F Natterer (Berlin: Springer) pp 127–39
- Natterer F 1986 *The Mathematics of Computerized Tomography* (Stuttgart: Wiley) pp 42–6
- Pélégriani M, de Dreuille O, Benali H, Bendriem B, Almeida P, Trebossen R, Buvat I and Di Paola R 1996 Fast quantitative measurement of attenuation map in SPECT using statistic-based sinogram regularization *J. Nucl. Med.* **37** 217P
- Radon J 1917 Über die Bestimmung von Funktionen durch ihre Integralwerte längs gewisser Mannigfaltigkeiten *Ber. Sächsische Akad. Wissenschaften, Lpz., Math.-Phys. Kl.* **69** 262–77
- Rao C R 1985 *Linear Statistical Inference and its Applications* (New York: Wiley) pp 357–8
- Reinsch C H 1967 Smoothing by spline functions *Numer. Math.* **10** 177–83
- Schoenberg I 1964 Spline functions and the problem of graduation *Proc. Natl Acad. Sci. USA* **52** 947–50
- Wahba G 1990 *Spline Models for Observational Data* (Philadelphia, PA: Society for Industrial and Applied Mathematics) pp 21–4
- Wold S 1978 Cross-validatory estimation of the number of components in factor and principal components models *Technometrics* **20** 397–405